J Nanostruct 15(4): 1520-1534, Autumn 2025

RESEARCH PAPER

# Removal of Rhodamine B from Aqueous Solutions Using Chitosan-g-poly(Acrylic Acid)/2-(((1E,2E)-1,2-Diphenyl-2-((4(E-1-(Thiazol 2ylimino) Ethyl) Phenyl) Imino) Ethylidene) Amino) Phenol Composite as an Adsorbent

*Makarim A. Mahdi* *, *Layth S. Jasim* *, *Hayder O. Jamel*

*Department of Chemistry, College of Education, University of Al-Qadisiyah, Diwaniyah, Iraq*

ARTICLE INFO

***Article History:***
*Received 05 June 2025*
*Accepted 14 August 2025*
*Published 01 October 2025*

***Keywords:***
*Adsorption*
*Rhodamine-B*
*Schiff base*
*Thermodynamic*

ABSTRACT

Based on the extensive research conducted, a composite, CS-g-PAA/DEAP, was developed and its physical and chemical properties were assessed. The composite's infrared spectroscopic profile depicted characteristic functional groups at specified frequency bands. Specific transformations in absorption bands demonstrated the composite's formation. Further changes upon Rh-B dye adsorption suggested significant interactions between the composite and the dye. Field Emission Scanning Electron Microscopy (FE-SEM) and Transmission Electron Microscopy (TEM) revealed altered surface characteristics of the composite after Schiff base integration, and distinct changes post-dye adsorption. Significant surface roughening, pore filling and particle agglomeration were noticed, indicating dye uptake. Thermogravimetric Analysis (TGA) revealed the thermal stability of the composite. Different decomposition stages were noticed at certain temperature ranges, suggesting the influence of nature of the monomers, crosslinking density, and functional groups on the thermal behavior of hydrogels. The effect of surface weight, pH, and temperature on dye adsorption was investigated. Adsorption decreased with increasing temperature, supporting the exothermic nature of the process. Also, a positive correlation between increased acidity and dye adsorption was observed. The thermodynamic functions suggested an exothermic and spontaneous adsorption process, with entropy reduction hinting at less randomness in adsorbed particles. Freundlich adsorption isotherm model was deemed suitable, indicating a multilayered, heterogeneous adsorption process. Further exploration of these properties would contribute to potential practical applications of the composite material.

**How to cite this article**
*Mahdi M., Jasim L., Jamel H. Removal of Rhodamine B from Aqueous Solutions Using Chitosan-g-poly(Acrylic Acid)/2-(((1E,2E)-1,2-Diphenyl-2-((4(E-1-(Thiazol 2ylimino) Ethyl) Phenyl) Imino) Ethylidene) Amino) Phenol Composite as an Adsorbent. J Nanostruct, 2025; 15(4):1520-1534. DOI: 10.22052/JNS.2025.04.003*

## INTRODUCTION

The increasing discharge of hazardous materials into water bodies due to various human activities has resulted in a critical global challenge – contemporary aquatic pollution [1]. This pollution has significant consequences for the environment, economy, and human health [2-4]. Among the major contributors to water toxicity are toxic

* *Corresponding Author Email: layth.alhayder@gmail.com*

metal ions and dyes, which have become more prevalent with industrial development [5]. These pollutants negatively impact aquatic life, interfere with plant enzymes, and necessitate immediate action to address this environmental threat and prevent numerous human diseases [6-9].

Rhodamine-B, a synthetic xanthene dye, is widely utilized in textiles, food, cosmetics, and other industries for its bright color, excellent solubility, and high photostability [10, 11]. Its strong absorbance and fluorescence properties make it suitable for various applications such as biological imaging, laser dyes, and tracing water flow in rivers and reservoirs [12]. However, the release of Rhodamine-B into the environment presents significant risks, including water pollution, aquatic life toxicity, and potential human health hazards [13]. Research has shown that Rhodamine-B can be toxic to various aquatic organisms, including fish, algae, and microorganisms, and can bioaccumulate in living organisms, leading to long-term health effects [14]. As a result, there is an urgent need for effective methods to remove Rhodamine-B from wastewater and reduce its environmental impact [15].

Chitosan (CS), a biopolymer derived from chitin, offers unique properties such as biodegradability, biocompatibility, non-toxicity, and excellent adsorption capacity, making it a promising candidate for pollutant removal [16-19]. However, the adsorption capacity of native chitosan is limited by its poor water solubility. To address this limitation, researchers have developed a composite material by grafting poly(acrylic acid) (PAA) chains onto the chitosan backbone, creating CS-g-p(AA)[20-23]. This modification significantly improves chitosan's solubility and adsorption capacity by introducing carboxyl groups that can form hydrogen bonds with target molecules [24]. Additionally, incorporating Schiff base moieties into the composite further enhances its adsorption capacity by providing more binding sites [25].

This article aims to offer an extensive overview of the adsorption process of Rhodamine-B onto CS-g-p(AA)/ DEAP composite surface, discussing its synthesis, characterization, and potential application in dye removal.

## MATERIALS AND METHODS

### *Instruments*

In this study, several instruments were employed, including a double-beam visible-ultraviolet spectrophotometer, a Fourier Transform Infrared Spectrometer (FTIR), a thermogravimetric analyzer, a FESEM, TEM, and a centrifuge. Additionally, an electric shaker was utilized.

### *Chemicals*

High-purity chemicals were used in this study, such as Acrylic acid (AA), Chitosan (CS), acetic acid, hydrochloric acid, sodium hydroxide, N,N-methylene-bis-acrylamide (MBA), potassium persulfate (KPS), 4-Aminoacetophenone, 2-aminothiazol, 4-amino-2-hydroxy benzoic acid, benzil, Glacial Acetic Acid and Rhodamine B (Rh-B) Fig. 1. All chemicals were supplied by Sigma Aldrich.

### *Preparation of Schiff base (DEAP) compound*

The compound (DEAP) was synthesized in two steps. The first step included the preparation of compound A, which is (E)-4-(1-(thiazo-2-ylimino) ethyl) aniline, which was prepared from dissolving (1.5 g, 1 mmol.) of 2-aminothiazol in (25 ml) of absolute ethanol and by continuing to stir, add to it (1.35 g, 1 mmol.) of 4-aminoacetophenone dissolved in (25 ml) of absolute ethanol. The mixture was refluxed for 8 hours, after which the mixture was cooled, and was observed that a precipitate formed, which was filtered and dried,

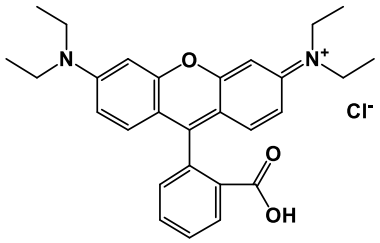


Fig. 1. The chemical structure of Rhodamine-B (Rh-B).

and then recrystallized from absolute ethanol and then the precipitate was collected, giving a product of (73%) and its melting point (207°C). As for the second step, included the preparation of compound (DEAP) by dissolving compound (A) in an amount of (2.1 g, 1 mmol.) in (15 ml) of absolute ethanol, and by continuous stirring, was added to it a solution (2.1 g, 1 mmol.) of benzil dissolved in (25 ml) of absolute ethanol and (1g, 1 mmol) of 2-aminophenol dissolved in (15 ml) of absolute ethanol and 4-5 drops of glacial acetic acid were added to the mixture. The mixture was refluxed for 8 hours; then, the mixture was cooled, where it was observed that a precipitate formed, which was filtered and dried, and recrystallized from absolute ethanol. The compound 2-(((1E,2E)-1,2-diphenyl-2-((4(E-1-(thiazol 2ylimino) ethyl) phenyl) imino) ethylidene) amino) phenol (DEAP) (Fig. 2) was obtained as solid orange yield 87%, m.p (227$^0$C).

*Preparation of Chitosan-g-poly(acrylic acid)/2-(((1E,2E)-1,2-diphenyl-2-((4(E-1-(thiazol 2ylimino) ethyl) phenyl) imino) ethylidene) amino) phenol composite*

Using the free radicals polymerization in an aqueous solution, by dissolving 0.5g of Chitosan (CS) in 20 mL from 1% acetic acid for 30 min with stirring and nitrogen gas for 15 min, the solution temperature was raised to 60° C with the added KPS (0.05g dissolved in 2 mL of distilled water) for 10 min with stirring, and nitrogen gas lasting for 10 min, after which the solution was cooled to 25 ° C, then add 5g of AA to above the solution with continuous stirring, after adding (0.1g) of DEAP for 15 min (dissolved in 2 ml ethanol) to the solution for 10 min; with continuous stirring, add (0.05g) of MBA (dissolved in 2ml distilled water) to the solution for 10 min, and stir with nitrogen gas for 20 min. This solution was transferred to plastic bottles and placed in a water bath at 60 ° C for three hr after the produced composite is cut into small pieces, washed with distilled water to remove interactive material, then dried in the oven at 70°C until a constant weight is obtained for further experiments Fig. 3.

*Product characterisation*

The prepared surface was characterized using Field Emission Scanning Electron Microscopy (FESEM), thermogravimetric analysis (TGA), and transmission electron microscopy (TEM), which were conducted in the Central Analytical Laboratory of KAC. Infrared spectroscopy (FTIR) analyses were carried out at the University of Al-Qadisiyah laboratories.

*Preparation of Standard (Rh-B) dye Solutions*

The standard solution of (Rh-B) dye used in this study was prepared at a concentration of 200 mg $L^{-1}$ by dissolving 0.2 g of the dye in one liter of deionized water. From this, various solutions with different concentrations were prepared.

*Determination of Maximum Wavelength and Calibration Curve for (Rh-B) dye*

The UV spectrum of (Rh-B) dye solutions in water at concentrations of 10 mg $L^{-1}$, was recorded. Absorption spectra were obtained using a UV/Vis spectrophotometer within the range of 200-800 nm with a 1 cm quartz cell. The λmax for (Rh-B) dye was found to be 554 nm. The calibration curve for (Rh-B) dye was determined by preparing a series of solutions with consecutive dilutions of the standard (Rh-B) dye solution at concentrations ranging from 1 to 10 mg $L^{-1}$, using a UV-Visible spectrophotometer. The absorbance of these solutions was recorded at the maximum

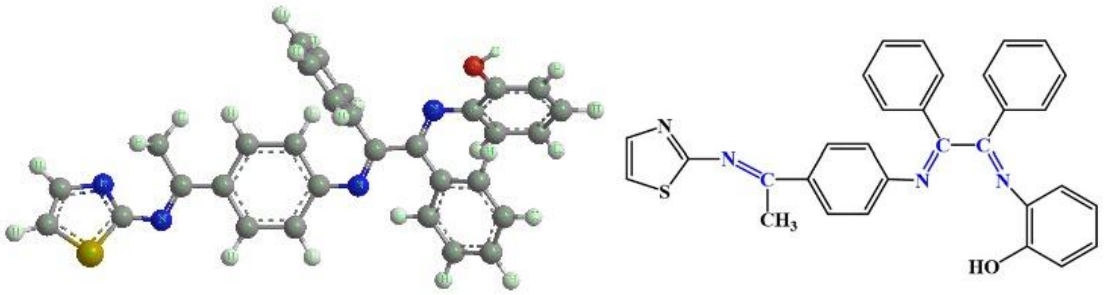


Fig.2. The proposed structural formula of compound (DEAP).

absorption wavelength of 554 nm for the dye[26]. A calibration curve was obtained by plotting the absorbance values against the concentrations. Effect of Adsorbent Weight on Adsorption

A series of weights ranging from 0.001 to 0.1 g of surface with 10 mL of dye solution (200 mg $L^{-1}$) [27]. The mixture was then placed in a shaker for 120 minutes at 25°C to reach equilibrium. Absorbance was measured after centrifugation at 6000 rpm for 15 minutes. The results were plotted as the amount adsorbed against the weight of the adsorbent to determine its effect on the adsorption process.

*Equilibrium Time for Adsorption Process*

The equilibrium time for dye adsorption on the adsorbent surface was determined by fixing all conditions, including temperature (25°C), pH, dye concentration, and surface weight, while varying the time factor [28]. A solution of 200 mg $L^{-1}$ (Rh-B) dye was prepared, and 10 mL of the dye solution was added to 0.05 g of the composite. The mixture was placed in a shaker at 25°C for varying durations (1-240 minutes). The absorbance of the solutions was measured after separation using a centrifuge to determine the optimal time for the adsorption process.

*Adsorption Isotherms*

Different concentrations of the dye (5-200 mg $L^{-1}$) were prepared, and 10 mL of each was added to 0.05 g of the adsorbent. The mixtures were placed in a shaker at a speed of 120 rotations per minute for 120 minutes for (Rh-B) dye at a temperature of 25°C. The samples were then centrifuged, and their absorbance was measured using a UV-Visible spectrophotometer. The quantity of (Rh-B) dye absorbed at equilibrium qe (mg $g^{-1}$), dye uptake, were determined using the following Eq. 1 [29-31]:

$$q_{e(\frac{mg}{g})} = \frac{V(C_o - C_e)}{m}$$

Where $C_o$ (mg $L^{-1}$) refers to the initial concentration of the dye, $C_e$ (mg $L^{-1}$) represents the dye concentration at equilibrium, V (L) stands for the solution volume, m (g) is the weight of CS-g-PAA/ DEAP. By employing equations (1), researchers can evaluate the effectiveness of dye adsorption using CS-g-PAA/ DEAP under various

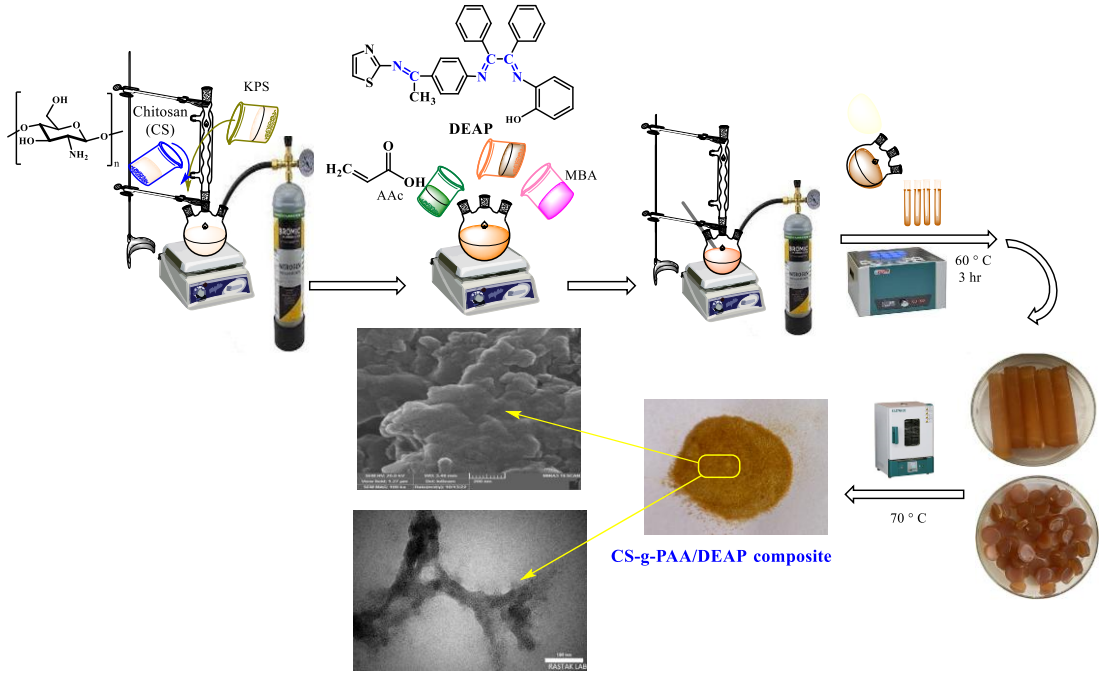


Fig. 3. illustrating the steps for preparing CS-g-PAA/DEAP composite.

experimental conditions.

*Effect of Temperature*

To determine the effect of temperature on the amount of substance adsorbed from aqueous solutions, the study was conducted on the (Rh-B) dye at temperatures ranging from 15, 20, 25, and 30°C. A 0.05 g of the composite was added to different concentrations (50-500 mg $L^{-1}$) for Rh-B in 10 mL of the dye solutions. The mixtures were placed in a shaker for 120 minutes for (Rh-B) dye, separated using a centrifuge, and the absorbance was measured using a UV-Visible spectrophotometer.

*Effect of Acidity Function*

The effect of acidity function on the adsorption process was studied by taking 0.05 gm of the surface and adding it to a dey solution with a concentration of 200 mg $L^{-1}$ for (Rh-B) dye at different acidity function values (2-10) at a temperature of 25°C and a duration of 120 minutes for (Rh-B) dye. The acidity function was adjusted using 0.1 M of hydrochloric acid solution and 0.1 M of sodium hydroxide solution, and the pH values were measured using a pH meter. The results were analyzed by plotting the amount of adsorbed substance against the acidity function value to determine its effect on the adsorption process.

## RESULTS AND DISCUSSION

*Characterization of the composite by FT-IR*

Infrared spectroscopy was utilized to diagnose the locations of functional group bands and to characterize the interatomic interactions. The FT-IR spectrum of CS-g-pAA Fig. 4a exhibited characteristic bands corresponding to the functional groups present in the polymer. The broad absorption band observed around 3420 $cm^{-1}$ was assigned to the stretching vibrations of -OH and -$NH_2$ groups in chitosan. The band at 1653 $cm^{-1}$ indicated the carbonyl stretching of the carboxylic acid groups in poly(acrylic acid), while the band around 1559 $cm^{-1}$ corresponded to the -$NH_2$ bending vibrations[32]. The FT-IR spectrum Fig. 4b of the Schiff base (DEAP) displayed characteristic bands associated with its molecular

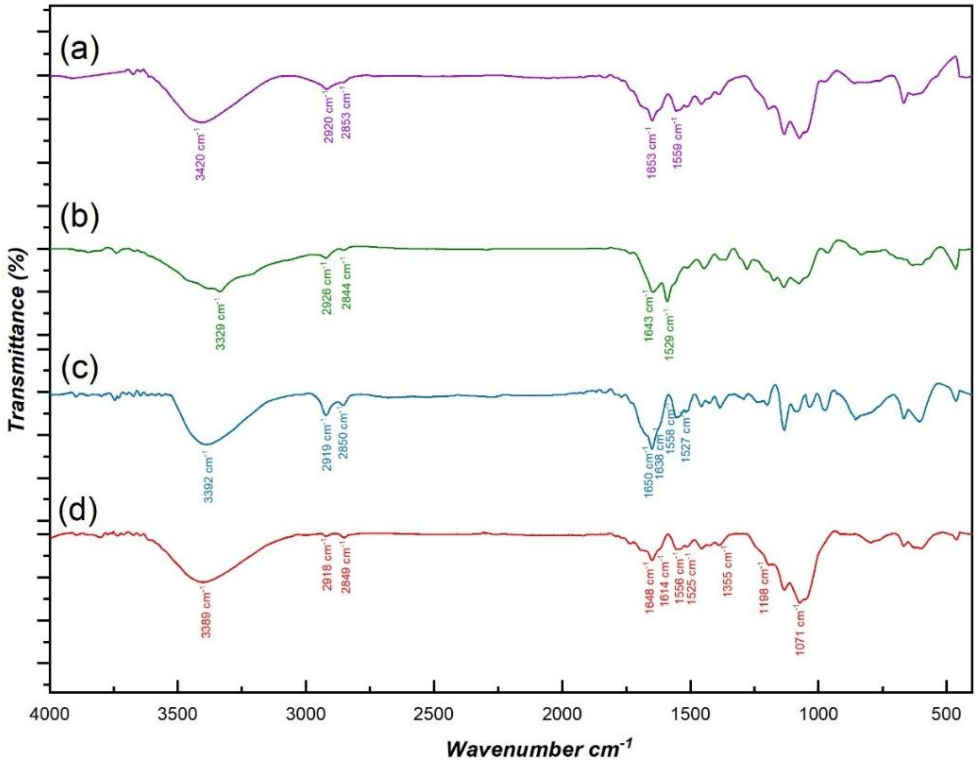


Fig. 4. FTIR Spectrum of the CS-g-PAA (a), DEAP (b)and CS-g-PAA/ DEAP before and after (Rh-B) dye adsorption(c,d).

structure. The absorption bands at 1643 $cm^{-1}$ and 1529 $cm^{-1}$ were attributed to the stretching vibrations of the C=N and C=C groups, respectively [33]. The presence of a broad absorption band around 3329 $cm^{-1}$ was indicative of the -OH group in the phenol moiety. The FT-IR spectrum Fig. 4c of the CS-g-PAA/ DEAP composite revealed the formation of the composite, as evidenced by the changes in the absorption bands compared to the individual components. A shift in the -OH and -$NH_2$ stretching vibrations to lower wavenumbers, along with a decrease in the intensity of the carbonyl stretching band, suggested the involvement of these functional groups in composite formation [34]. Additionally, the appearance of a new band at 1527 $cm^{-1}$ indicated the presence of the coordinated Schiff base (DEAP). The FTIR spectra Fig. 4d of the CS-g-PAA/DEAP composite after (Rh-B) dye adsorption revealed significant changes in the characteristic absorption bands, indicating interactions between the adsorbent and (Rh-B) dye. The FTIR peaks of (Rh-B) dye after adsorption onto the CS-g-PAA/DEAP appear at 1198 and 1355 $cm^{-1}$ which are assigned as C-O-C and C-aryl of RhB molecules. Because of the adsorption of Rh-B dye on the CS-g-PAA/ DEAP composite, the stretching vibration of the C–H bond was changed from 2920 $cm^{-1}$ to 2918 $cm^{-1}$.Moreover, the C-N peak of (Rh-B) dye after adsorption is observed at 1614 $cm^{-1}$ which relates the electrostatic adsorption between (Rh-B) dye and composite. In addition to this, FTIR peaks from 1525 to 1355 $cm^{-1}$ are due to the aromatic ring structure and red-shifted from pure (Rh-B) dye due to π-π interaction [35]. FTIR spectra reveal the main interacting forces like π-π interaction and electrostatic interaction/ hydrogen bonding [36-39].

*FESEM and TEM analyses*

The Field Emission Scanning Electron Microscopy (FE-SEM) technique was employed to investigate the surface characteristics of synthesized materials, enabling the assessment of particle shape, size, aggregation, and surface nature (porous or smooth). Furthermore, it facilitated the examination of component homogeneity, distribution on the surface, and interconnection of polymer chains [40]. Upon incorporating the Schiff base (DEAP) into the hydrogel, the resulting composite, CS-g-PAA/DEAP Fig. 5a, demonstrated a morphological alteration characterized by increased roughness, porosity, and irregular structure. The reagent molecules were homogeneously dispersed throughout the

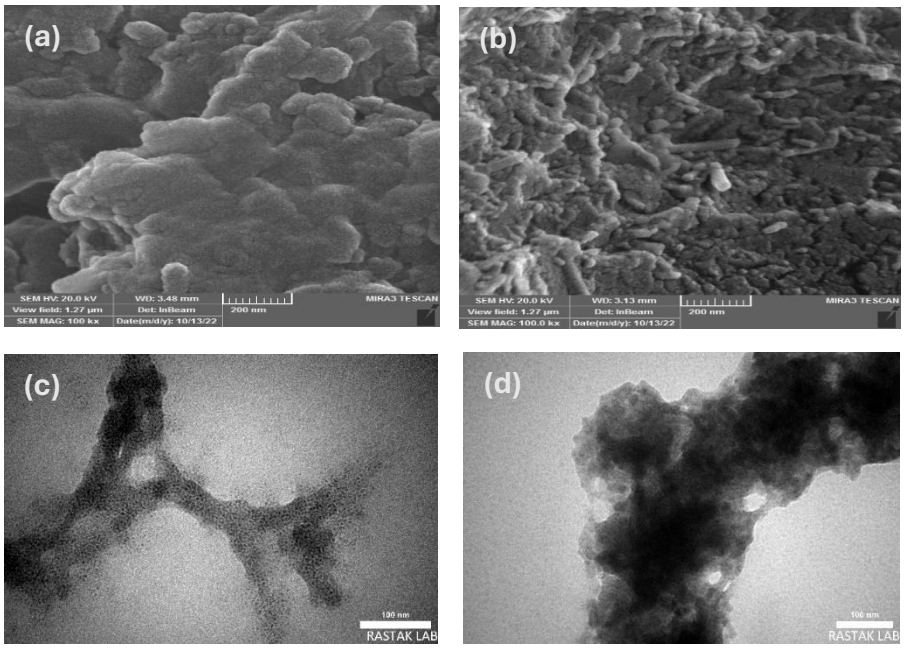


Fig. 5. FESEM and TEM of composite before (a and c), and after adsorption of (Rh-B) dye (b and c).

hydrogel matrix [41]. The absence of Schiff base aggregations can be ascribed to the interfacial interaction between the schiff base and the hydrogel matrix, facilitated by the functional groups present on both the DEAP and hydrogel surfaces.

Concerning the adsorption of rhodamine dye on CS-g-PAA/ DEAP composite, the FE-SEM images in Fig. 5b indicate an increase in surface smoothness resulting from the complete filling of surface pores by dye molecules. Consequently, the surface becomes entirely covered by the dye molecules, confirming the adsorption process.

The TEM images reveal valuable insights into the surface composition and response to the adsorption process [42]. The TEM analysis depicted in Fig. 5c demonstrates that CS-g-PAA/ DEAP composite exhibit small, dispersed particles that are uniformly distributed and regularly arranged [43]. Additionally, the presence of some agglomerates is noted. The surfaces are characterized by the formation of thin layers, which contribute to their overall structure.

Upon the occurrence of the adsorption process, several changes in surface morphology are observed. Firstly, an increased presence of agglomerates with larger sizes is detected [44]. This phenomenon is attributed to the interference between dye molecules and surface molecules during the adsorption process [45]. Secondly, the thin layers of overlying materials diminish, likely due to the absorption and accumulation of dye molecules that penetrate the pores and grooves on the surface. The penetrating Transmission Electron Microscope (TEM) technique proves to be an effective method for analyzing the properties of surface CS-g-PAA/DEAP composite. The findings highlight the uniform distribution of particles, the presence of thin layers, and the changes in surface morphology upon the adsorption process Fig. 5d. Further research is recommended to explore the implications of these observations on the functional properties of the materials under investigation [46].

*Thermo gravimetric Analysis (TGA)*

TGA curve showed from Fig. 6, where the sample was heated in the presence of nitrogen gas within the temperature range of 40-800°C at a rate of 10°C.min$^{-}$1. The TGA curve of Schiff base (DEAP) exhibited a multi-step decomposition process, indicating the presence of different decomposition stages with varying mass loss profiles[47]. The initial mass loss stage, observed between 100-250°C, can be attributed to the loss of volatile components, such as water or solvent molecules. Subsequent mass loss stages, observed between 250-600°C, are attributed to the decomposition of the compound's organic moieties, including phenol, imine, and thiazole groups [48]. The final mass loss stage, observed above 600°C, corresponds to the complete decomposition of DEAP and the formation of residual char. The thermal characteristics of CS-g-PAA and CS-

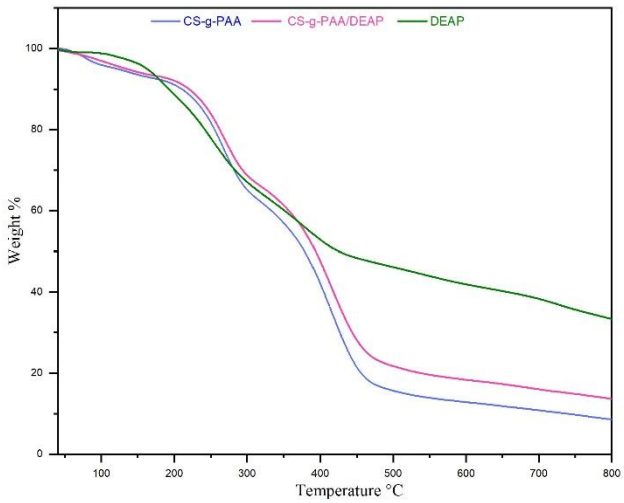


Fig. 6. TGA Curve of the DEA ,CS-g-PAA and CS-g-PAA/ DEAP.

g-PAA/DEAP composite demonstrated similar degradation profi les with curves disintegrated in three steps. The first degradation occurred in the temperature range of 60–200 °C due to the loss of water residual. In the temperature region of 200–300°C, there was a second decomposition stage of due to degradation of CS. In the third degradation profile in weight reduction occurred in the temperature range of 300–500°C due to the breaking of its carboxyl from acrylic acid groups and degradation of the residual polymer [49]. The TGA curves revealed that the thermal stability and decomposition behavior of hydrogels are strongly influenced by factors such as the nature of the

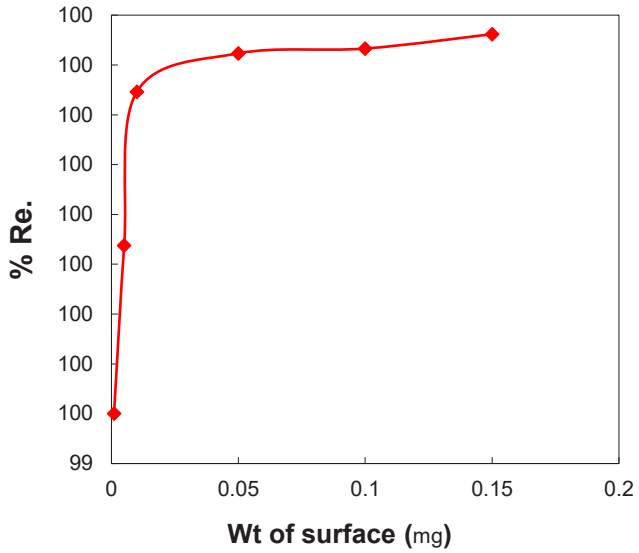


Fig. 7. The effect of surface weight on the adsorption of (Rh-B) dye at 25°C.

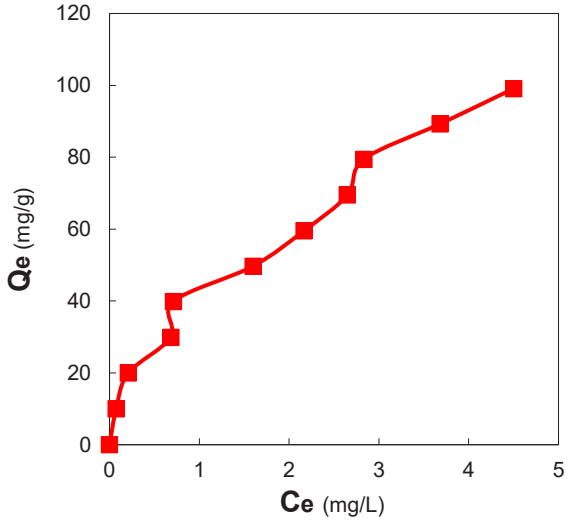


Fig. 8. The adsorption isotherm of (Rh-B) dye on the CS-g-PAA/DEAP composite.

monomers, crosslinking density, and the presence of functional groups [50]. The TGA results showed a significant improvement in the thermal stability of the CS-g-PAA/ DEAP composite hybrid materials compared to the pristine CS-g-PAA.

*Effect of Surface Weight*

The effect of surface weight on the removal of (Rh-B) dye has been studied by utilizing varying weights of the adsorbent material at a constant concentration of (Rh-B) dye (200 mg $L^{-1}$) at 25°C Fig. 7. The findings of the study are presented in Fig. 6, which illustrates the impact of surface weight on the adsorption of (Rh-B) dye at 25°C and a pH of 7.

*Factors that affect the adsorption of dye*

The adsorption isotherm for the (Rh-B) dye was calculated on the surface of the CS-g-PAA/ DEAP composite. The results demonstrated that the adsorption process corresponds to the $S_4$ category according to the Giles Classification, as illustrated in Fig. 8. In this category, the adsorbed molecules tend to orient themselves perpendicularly or obliquely on the adsorbent surface [51]. This type of orientation indicates the occurrence of multilayer adsorption due to the heterogeneous nature of the surface [52].

*Effect of the temperature*

The results, as shown in Fig. 9, demonstrate that the amount of dye adsorbed on the surface of the composite decreased with increasing temperature, indicating that the adsorption process is exothermic [53]. This is attributed to the fact that rising temperatures reduce the adsorption of dye on the absorbent surface by increasing the solubility of adsorbed dye particles in the solvent. On the other hand, an increase in temperature also increases the kinetic energy of the adsorbed particles, which in turn increases the randomness in the system (increase in system entropy ΔS), thereby weakening the attraction between dye molecules and active sites on the absorbent surface [54-56].

Thermodynamic function values are of great importance since they explain many reactions, particularly in the adsorption process. They enable the determination of the reaction direction and the nature of the controlling forces, and provide a good description of the regularity of the molecules resulting from molecular interactions. The enthalpy change (ΔH) value represents a measure to identify the interaction forces between the adsorbed dye molecules and the adsorbing surface[57]. By plotting lnXm versus the inverse of absolute temperature 1000/T, as shown

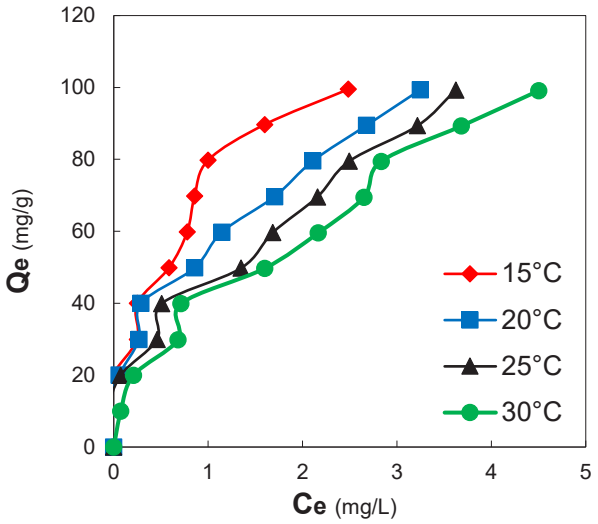


Fig. 9. Effect of Temperature on (Rh-B) Dye Adsorption by Composite Surface at Different Temperatures (t=120 min, V=10 mL, wt=0.05).

in Table 1 and Fig. 10, a linear relationship is obtained, and the enthalpy change (ΔH) value for (Rh-B) dye adsorption on the composite surface is determined.

The thermodynamic functions have been calculated to interpret the adsorption processes of Rh-B dye on the surface of the composite. Table 2 presents the thermodynamic function values for the dye adsorption process on the composite surface. The negative sign of the change in enthalpy (ΔH) implies that the adsorption process is exothermic due to the disruption and dissociation of bonds that form between the active centers of the absorbent surface and dye particles, i.e., the adsorption process will decrease with increasing temperature. Meanwhile, the negative value for the change in entropy (ΔS) signifies a reduction in the randomness of the adsorbed particles, meaning they will become less ordered[11, 58]. The results also showed that the adsorption process occurred spontaneously under the reaction conditions, as indicated by the negative value for the Gibbs free energy (ΔG) [59-64].

Langmuir, Freundlich, and Temkin adsorption models have been applied to describe the adsorption properties of the adsorbents used in the removal of pollutants, as seen in Table 3 and Fig. 11. It appears that the adsorption of Rh-B dye on the surface of the composite is consistent with the Freundlich model [65-70]. This is clearly demonstrated by the correlation coefficient (R2) for the dye on the composite surface, which equals 0.9749.

The applicability of the Freundlich isotherm to the adsorption of Rh-B dye on the composite

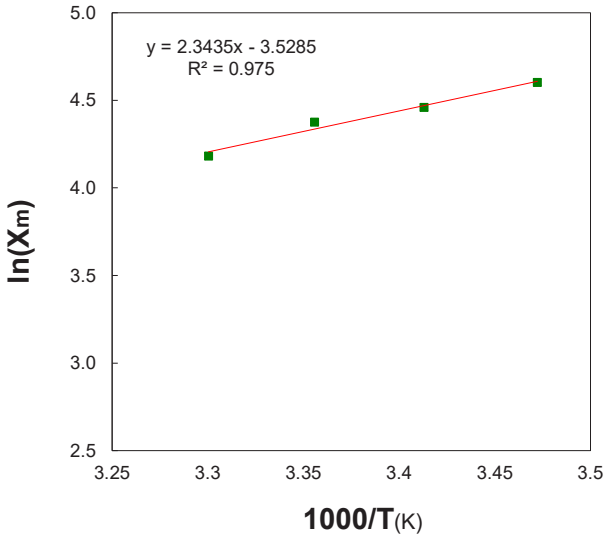


Fig. 10. A plot of lnXm vs. Inverse Absolute Temperature for (Rh-B) dye Adsorption on composite Surface.

Table 1. The effect of temperature on the maximum adsorbed amount for the adsorption of (Rh-B) dye on the surface of the composite.

| Temperature(°C) | Temperature(K) | $1/T_{(K)}$ | $1000/T_{(K)}$ | $C_e$ | $X_m$ | $\ln X_m$ |
|---|---|---|---|---|---|---|
| 15 | 288 | 0.003472 | 3.472222 | 2.4 | 99.7 | 4.602165677 |
| 20 | 293 | 0.003413 | 3.412969 | 2.4 | 86.5 | 4.460144414 |
| 25 | 298 | 0.003356 | 3.355705 | 2.4 | 79.5 | 4.375757022 |
| 30 | 303 | 0.0033 | 3.30033 | 2.4 | 65.5 | 4.182050143 |

surface indicates the heterogeneous nature of the surface and that the active sites on the composite surface have unequal energies. It also suggests that the adsorption is not confined to a single molecular layer, but is multilayered [71-73].

*Effect of pH*

In this study, the impact of acidity on the adsorption process of Rhodamine B dye on the surface of the CS-g-PAA/ DEAP composite was investigated. The dye concentration was fixed at

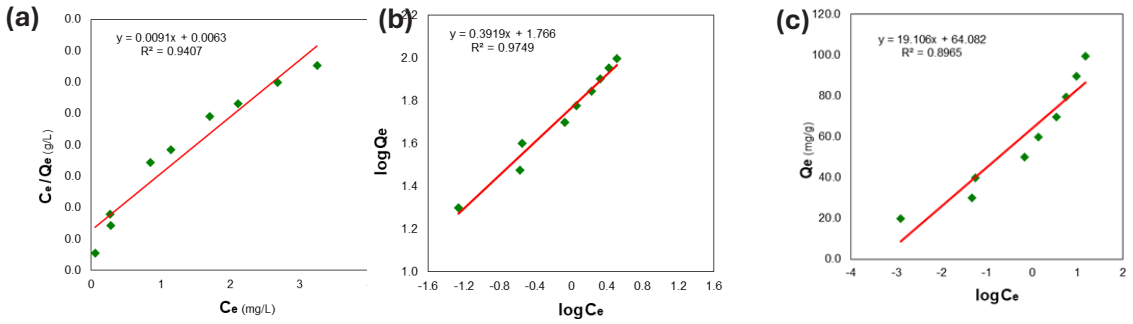


Fig. 11. Langmuir(a), Freundlich(b), and Temkin(c) isotherms for adsorption of Rh-B dye on the adsorbent surface.

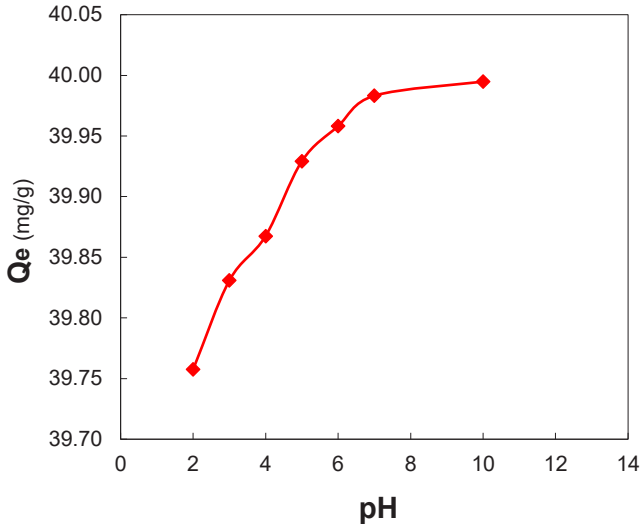


Fig. 12. Effect of Acid Function on Rhodamine B Adsorption (t=120 min, V=10 mL, wt=0.05, C=200mg $L^{-1}$, T=25°C).

Table 2. Correlation coefficients an d constants for Langmuir, Freundlich, and Temkin isotherms for Rh-B dye adsorption on the surfaces of the adsorbing composites.

| Langmuir | | | Freundlich | | | Timken | | |
|---|---|---|---|---|---|---|---|---|
| $K_L$ | $q_m$ | $R^2$ | $K_F$ | n | $R^2$ | $K_T$ | b | $R^2$ |
| 1.4444 | 109.8901 | 0.9407 | 58.3445 | 2.5516 | 0.9749 | 28.6176 | 19.106 | 0.8965 |

200 ppm, and different pH values ranging from 2 to 10 were considered. The other variables, such as time and temperature, were held constant. As depicted in Fig. 12, acidity was found to have a significant effect on the adsorbent material and the composite surface, as well as on the interactions between them. It was observed that the dye adsorption on the composite surface increased with increasing acidity [74]. This can be attributed to Rhodamine B being a cationic dye [75]. At low pH values, the concentration of H+ ions in the solution is very high, leading to competitive interactions between the dye molecules and the H+ ions for the active sites on the composite surface. This results in a decrease in adsorption. Furthermore, the composite surface contains carbonyl, carboxyl, and hydroxyl groups. At low pH values, these groups are protonated, leading to hydrogen bonding between the chains and causing the composite surface to shrink. This makes it difficult for the dye molecules to diffuse into the composite surface. Additionally, electrostatic repulsion occurs between the COOH and OH groups on the surface and the positively charged dye, making it difficult for the dye molecules to access the active sites on the surface and reducing adsorption[76]. On the other hand, at high pH values, the carboxyl and hydroxyl groups on the composite surface deprotonate and become negatively charged. This leads to the electrostatic attraction between the negatively charged surface and the positively charged dye molecules, resulting in increased adsorption.[77] Moreover, at high pH values, the negatively charged functional groups on the composite surface repel each other, causing swelling and expansion. This allows the dye molecules to diffuse into the composite surface, thereby increasing adsorption [78].

## CONCLUSION

Based on the experimental study, the CS-g-PAA/DEAP composite surface effectively adsorbed Rhodamine B from its aqueous solution with an optimal equilibrium time of 120 minutes. The adsorption process was found to be exothermic and influenced by acidity. The adsorption of Rhodamine B occurred spontaneously on the composite surface, with Rhodamine B showing a negative entropy change. The adsorption of Rhodamine-B onto CS-g-pAA/DEAP composite surfaces has demonstrated promising potential for the removal of dyes and other pollutants from wastewater. The unique properties of these composites, including their enhanced solubility, adsorption capacity, and affinity towards dye molecules, make them ideal candidates for various wastewater treatment applications. By understanding the synthesis, characterization, and adsorption mechanisms of these materials, researchers can continue to develop novel and efficient adsorbents for environmental remediation and sustainable development.

## CONFLICT OF INTEREST

The authors declare that there is no conflict of interests regarding the publication of this manuscript.

## REFERENCES

1. Yagub MT, Sen TK, Afroze S, Ang HM. Dye and its removal from aqueous solution by adsorption: A review. Advances in Colloid and Interface Science. 2014;209:172-184.
2. Shi Y, Chang Q, Zhang T, Song G, Sun Y, Ding G. A review on selective dye adsorption by different mechanisms. Journal of Environmental Chemical Engineering. 2022;10(6):108639.
3. Zeeshan M, Javed T, Kumari C, Thumma A, Wasim M, Taj MB, et al. Investigating the interactions between dyes and porous/composite materials: A comprehensive study. Sustainable Chemistry for the Environment. 2025;9:100217.
4. N. Zghair A, T. Al-Khateeb Z, S. Jasim L, Batool M. Synthesis, characterization and adsorption properties of azo-functionalized polymeric hydrogels for R6G dye removal from water. Applied Chemical Engineering. 2025;8(1).
5. Ma X, Zhao S, Tian Z, Duan G, Pan H, Yue Y, et al. MOFs meet wood: Reusable magnetic hydrophilic composites toward efficient water treatment with super-high dye adsorption capacity at high dye concentration. Chem Eng J. 2022;446:136851.
6. Basar C. Applicability of the various adsorption models of three dyes adsorption onto activated carbon prepared waste apricot. J Hazard Mater. 2006;135(1-3):232-241.
7. Qasim SM, Al-Khateeb ZT, Jabbar FA, Batool M, Jasim LS. Adsorptive and reactivation potential of clay based superabsorbent kappa (κ)-carrageenan-graft-poly (acrylic acid-co-acrylamide)/ kaolin composite for malachite green dye: Linear and non-linear modeling. J Mol Struct. 2025;1348:143448.
8. Saadallah K, Ad C, Djedid M, Batool M, Benalia M, Saadallah S, et al. Potential of the Algerian pine tree bark for the adsorptive removal of methylene blue dye: Kinetics, isotherm and mechanism study. J Dispersion Sci Technol. 2024:1-19.
9. Nano Modifications of Biochar to Enhance Heavy Metal Adsorption from Wastewaters: A Review. American Chemical Society (ACS).
10. Saruchi, Kumar V. Adsorption kinetics and isotherms for the removal of rhodamine B dye and Pb+2 ions from aqueous solutions by a hybrid ion-exchanger. Arabian Journal of Chemistry. 2019;12(3):316-329.
11. Jamel HO, Jasim MH, Mahdi MA, Ganduh SH, Batool M, Jasim LS, et al. Adsorption of Rhodamine B dye from

solution using 3-((1-(4-((1H-benzo[d]imidazol-2-yl)amino) phenyl)ethylidene)amino)phenol (BIAPEHB)/ P(AA-co-AM) composite. Desalination and Water Treatment. 2025;321:101019.
12. Amalina F, Abd Razak AS, Krishnan S, Zularisam AW, Nasrullah M. A review of eco-sustainable techniques for the removal of Rhodamine B dye utilizing biomass residue adsorbents. Physics and Chemistry of the Earth, Parts A/B/C. 2022;128:103267.
13. Kumar R, Dey R, Kalita T, Pariyal S, Sankar Goswami B, Haldar J, et al. Engineering a unique Multi-tasking polymer that specifically prevents rhodamine B and fluoride ion toxicity with Anti-bacterial responses against MRSA. Eur Polym J. 2022;176:111401.
14. Tkaczyk A, Mitrowska K, Posyniak A. Synthetic organic dyes as contaminants of the aquatic environment and their implications for ecosystems: A review. Sci Total Environ. 2020;717:137222.
15. Skjolding LM, Jørgensen Lv, Dyhr KS, Köppl CJ, McKnight US, Bauer-Gottwein P, et al. Assessing the aquatic toxicity and environmental safety of tracer compounds Rhodamine B and Rhodamine WT. Water Res. 2021;197:117109.
16. Pillai CKS, Paul W, Sharma CP. Chitin and chitosan polymers: Chemistry, solubility and fiber formation. Prog Polym Sci. 2009;34(7):641-678.
17. Ali MM, Mhaibes RM, Othman MA-M, R. Lahhob Q, Qasim MJ. Association between triglyceride-glucose index and risk of chronic kidney disease: a systematic review and meta-analysis. Journal of Nephropharmacology. 2024;13(2):e12692.
18. Hashim Al-Zuhairy S, Abed Darweesh M, Abdul-Mounther Othman M, Al-Huda Salah Al-Zuhairy N. Vitamin D deficiency in young children with iron deficiency in Misan province, Iraq. J Med Life. 2022;15(3):387-391.
19. Hmood NA, Mother Othman DMA, Mohsin Ali DM. Transcription Factor 7-Like 2 Gene Polymorphisms rs7903146associationwith Type 2 Diabetic Polycystic Ovarian Syndrome Women of Iraqi Population. Annals of Tropical Medicine and Public Health. 2019;22(12):156-164.
20. Hu Y, Jiang X, Ding Y, Ge H, Yuan Y, Yang C. Synthesis and characterization of chitosan–poly(acrylic acid) nanoparticles. Biomaterials. 2002;23(15):3193-3201.
21. Synthesis and Characterization of Novel Compounds Derived From 6-methyl-2,6 dihydro[1,2,4-triazino[4,3-b] indazol-3(4H)-one. International Journal of Pharmaceutical Research. 2020;12(sp1).
22. Al-Suraify SMT, Hussien LB. Retraction Note: Synthesis and characterization of new compounds derived from 1H-indol-5-ylamine. Applied Nanoscience. 2024;14(4):719-719.
23. Synthesis of New Nitrogenous Derivatives Based On 3-Chloro–1-methyl-1H-indazole. International Journal of Pharmaceutical Research. 2020;12(sp1).
24. Torrado S. Chitosan-poly(acrylic) acid polyionic complex: in vivo study to demonstrate prolonged gastric retention. Biomaterials. 2004;25(5):917-923.
25. Antony R, Arun T, Manickam STD. A review on applications of chitosan-based Schiff bases. Int J Biol Macromol. 2019;129:615-633.
26. Yu M, Gao M, Shen T, Zeng H. Single and simultaneous adsorption of rhodamine B and congo red from aqueous solution by organo-vermiculites. J Mol Liq. 2019;292:111408.
27. Tang L, Cai Y, Yang G, Liu Y, Zeng G, Zhou Y, et al. Cobalt nanoparticles-embedded magnetic ordered mesoporous carbon for highly effective adsorption of rhodamine B. Appl Surf Sci. 2014;314:746-753.
28. Ding L, Zou B, Gao W, Liu Q, Wang Z, Guo Y, et al. Adsorption of Rhodamine-B from aqueous solution using treated rice husk-based activated carbon. Colloids Surf Physicochem Eng Aspects. 2014;446:1-7.
29. Wanyonyi WC, Onyari JM, Shiundu PM. Adsorption of Congo Red Dye from Aqueous Solutions Using Roots of Eichhornia Crassipes: Kinetic and Equilibrium Studies. Energy Procedia. 2014;50:862-869.
30. Javed T, Kausar F, Zawar MD, Khalid N, Thumma A, Ismail A, et al. Investigating the adsorption potential of coconut coir as an economical adsorbent for decontamination of lanthanum ion from aqueous solution. J Dispersion Sci Technol. 2024:1-12.
31. Urooj H, Javed T, Taj MB, Nouman Haider M. Adsorption of crystal violet dye from wastewater on Phyllanthus emblica fruit (PEF) powder: kinetic and thermodynamic. Int J Environ Anal Chem. 2023;104(19):7474-7499.
32. Lin Y, Hong Y, Song Q, Zhang Z, Gao J, Tao T. Highly efficient removal of copper ions from water using poly(acrylic acid)-grafted chitosan adsorbent. Colloid Polym Sci. 2017;295(4):627-635.
33. Amorim CR, Pavani TFA, Lopes AFS, Duque MD, Mengarda ACA, Silva MP, et al. Schiff bases of 4-Phenyl-2-Aminothiazoles as hits to new antischistosomals: Synthesis, in vitro, in vivo and in silico studies. Eur J Pharm Sci. 2020;150:105371.
34. Fookes FA, Mengatto LN, Rigalli A, Luna JA. Controlled fluoride release for osteoporosis treatment using orally administered chitosan hydrogels. J Drug Deliv Sci Technol. 2019;51:268-275.
35. Malik SA, Dar AA, Banday JA. Rheological, morphological and swelling properties of dysprosium-based composite hydrogel beads of alginate and chitosan: A promising material for the effective cationic and anionic dye removal. Colloids Surf Physicochem Eng Aspects. 2023;663:131046.
36. Adly MS, El-Dafrawy SM, El-Hakam SA. Application of nanostructured graphene oxide/titanium dioxide composites for photocatalytic degradation of rhodamine B and acid green 25 dyes. Journal of Materials Research and Technology. 2019;8(6):5610-5622.
37. Batool M, Haider MN, Javed T. Applications of Spectroscopic Techniques for Characterization of Polymer Nanocomposite: A Review. Journal of Inorganic and Organometallic Polymers and Materials. 2022;32(12):4478-4503.
38. Bukhari A, Javed T, Haider MN. Adsorptive exclusion of crystal violet dye from wastewater by using fish scales as an adsorbent. J Dispersion Sci Technol. 2022;44(11):2081-2092.
39. Haider MN. Enhanced degradation of reactive violet 1 (RV1) dye using gamma and UV irradiation Coupled with hydrogen peroxide. Radiat Phys Chem. 2026;238:113191.
40. Falsafi SR, Rostamabadi H, Assadpour E, Jafari SM. Morphology and microstructural analysis of bioactive-loaded micro/nanocarriers via microscopy techniques; CLSM/SEM/TEM/AFM. Advances in Colloid and Interface Science. 2020;280:102166.
41. Yu J, Lu Q, Zheng J, Li Y. Chitosan/attapulgite/poly(acrylic acid) hydrogel prepared by glow-discharge electrolysis plasma as a reusable adsorbent for selective removal of $Pb^{2+}$ ions. Iranian Polymer Journal. 2019;28(10):881-893.

42. Abou Taleb MF, Abou El Fadl FI, Albalwi H. Adsorption of toxic dye in wastewater onto magnetic NVP/CS nanocomposite hydrogels synthesized using gamma radiation. Sep Purif Technol. 2021;266:118551.
43. Zhang C, Dai Y, Wu Y, Lu G, Cao Z, Cheng J, et al. Facile preparation of polyacrylamide/chitosan/$Fe_3O_4$ composite hydrogels for effective removal of methylene blue from aqueous solution. Carbohydr Polym. 2020;234:115882.
44. Ali HE, Nasef SM, Gad YH. Remediation of Astrazon blue and Lerui acid brilliant blue dyes from waste solutions using amphoteric superparamagnetic nanocomposite hydrogels based on chitosan prepared by gamma rays. Carbohydr Polym. 2022;283:119149.
45. Xu P, Zheng M, Chen N, Wu Z, Xu N, Tang J, et al. Uniform magnetic chitosan microspheres with radially oriented channels by electrostatic droplets method for efficient removal of Acid Blue. Journal of the Taiwan Institute of Chemical Engineers. 2019;104:210-218.
46. Jamali M, Akbari A. Facile fabrication of magnetic chitosan hydrogel beads and modified by interfacial polymerization method and study of adsorption of cationic/anionic dyes from aqueous solution. Journal of Environmental Chemical Engineering. 2021;9(3):105175.
47. Dawar N, Devi J, Kumar B, Dubey A. Synthesis, Characterization, Pharmacological Screening, Molecular Docking, DFT, MESP, ADMET Studies of Transition Metal(II) Chelates of Bidentate Schiff Base Ligand. Inorg Chem Commun. 2023;151:110567.
48. Varshney A, Mishra AP. Synthesis, spectral characterization, computational studies, antifungal, DNA interaction, antioxidant and fluorescence property of novel Schiff base ligand and its metal chelates. Spectrochimica Acta Part A: Molecular and Biomolecular Spectroscopy. 2023;297:122765.
49. Sethy TR, Pradhan AK, Sahoo PK. Simultaneous studies on kinetics, bio-adsorption behaviour of chitosan grafted thin film nanohydrogel for removal of hazardous metal ion from water. Environmental Nanotechnology, Monitoring & Management. 2019;12:100262.
50. Zeng T, Hu X-q, Wu H, Yang J-w, Zhang H-b. Microwave assisted synthesis and characterization of a novel bio-based flocculant from dextran and chitosan. Int J Biol Macromol. 2019;131:760-768.
51. Morais da Silva PM, Camparotto NG, Grego Lira KT, Franco Picone CS, Prediger P. Adsorptive removal of basic dye onto sustainable chitosan beads: Equilibrium, kinetics, stability, continuous-mode adsorption and mechanism. Sustainable Chemistry and Pharmacy. 2020;18:100318.
52. Stanciu MC, Nichifor M. Influence of dextran hydrogel characteristics on adsorption capacity for anionic dyes. Carbohydr Polym. 2018;199:75-83.
53. Foroutan R, Peighambardoust SJ, Esvandi Z, Khatooni H, Ramavandi B. Evaluation of two cationic dyes removal from aqueous environments using CNT/MgO/$CuFe_2O_4$ magnetic composite powder: A comparative study. Journal of Environmental Chemical Engineering. 2021;9(2):104752.
54. Ali F, Ali N, Bibi I, Said A, Nawaz S, Ali Z, et al. Adsorption isotherm, kinetics and thermodynamic of acid blue and basic blue dyes onto activated charcoal. Case Studies in Chemical and Environmental Engineering. 2020;2:100040.
55. Arshad R, Javed T, Thumma A. Exploring the efficiency of sodium alginate beads and Cedrus deodara sawdust for adsorptive removal of crystal violet dye. J Dispersion Sci Technol. 2023;45(12):2330-2343.
56. Majeed HJ, Idrees TJ, Mahdi MA, Abed MJ, Batool M, Yousefi SR, et al. Synthesis and application of novel sodium carboxy methyl cellulose-g-poly acrylic acid carbon dots hydrogel nanocomposite (NaCMC-g-PAAc/ CDs) for adsorptive removal of malachite green dye. Desalination and Water Treatment. 2024;320:100822.
57. Gharbani P, Mehrizad A. Preparation and characterization of graphitic carbon nitrides/polyvinylidene fluoride adsorptive membrane modified with chitosan for Rhodamine B dye removal from water: Adsorption isotherms, kinetics and thermodynamics. Carbohydr Polym. 2022;277:118860.
58. Wang J, Ding L, Wei J, Liu F. Adsorption of copper ions by ion-imprinted simultaneous interpenetrating network hydrogel: Thermodynamics, morphology and mechanism. Appl Surf Sci. 2014;305:412-418.
59. Katal R, Baei MS, Rahmati HT, Esfandian H. Kinetic, isotherm and thermodynamic study of nitrate adsorption from aqueous solution using modified rice husk. Journal of Industrial and Engineering Chemistry. 2012;18(1):295-302.
60. Shah A, Arjunan A, Manning G, Batool M, Zakharova J, Hawkins AJ, et al. Sequential novel use of Moringa oleifera Lam., biochar, and sand to remove turbidity, E. coli, and heavy metals from drinking water. Cleaner Water. 2024;2:100050.
61. Shah A, Arjunan A, Thumma A, Zakharova J, Bolarinwa T, Devi S, et al. Adsorptive removal of arsenic from drinking water using KOH-modified sewage sludge-derived biochar. Cleaner Water. 2024;2:100022.
62. Mahdi MA, Oroumi G, Samimi F, Dawi EA, Abed MJ, Alzaidy AH, et al. Tailoring the innovative $Lu_2CrMnO_6$ double perovskite nanostructure as an efficient electrode materials for electrochemical hydrogen storage application. Journal of Energy Storage. 2024;88:111660.
63. Sahoo R, Sahoo S, Azizi S. Tamarind seed polysaccharides and their nanocomposites for drug delivery: An economical, eco-friendly and novel approach. Manipal Journal of Medical Sciences. 2017;2(2).
64. Mahde BW, Sultan AM, Mahdi MA, Jasim LS. Kinetic Adsorption and Release Study of Sulfadiazine Hydrochloride Drug from Aqueous Solutions on GO/P(AA-AM-MCC) Composite. International Journal of Drug Delivery Technology. 2022;12(04):1583-1589.
65. Zhang W, Yang G, Deng F, Liang J, Huang Q, Dou J, et al. Direct grafting of cellulose nanocrystals with poly(ionic liquids) via Gamma-ray irradiation and their utilization for adsorptive removal of CR. Int J Biol Macromol. 2022;194:1029-1037.
66. Mittal H, Al Alili A, Alhassan SM. High efficiency removal of methylene blue dye using κ-carrageenan-poly(acrylamide-co-methacrylic acid)/AQSOA-Z05 zeolite hydrogel composites. Cellulose. 2020;27(14):8269-8285.
67. Irhayyim SH, Jasim LS. Synthesis, characterisation and application of novel sodium alginate-itaconic acid-acrylic acid-bentonite (SA-IA-AAc-bentonite) composite for metoprolol (MTP) adsorption from water. Int J Environ Anal Chem. 2025:1-37.
68. Al-Adilee KJ, Atyha SA. Synthesis, Spectral, Thermal and Biological Studies of Some Metal Complexes Derived from Heterocyclic Mono Azo Dye Ligand 2'[(2'-Hydroxy-4-methyl phenyl)azo]imidazole. Asian J Chem. 2018;30(2):280-292.
69. Jabbar FA, Jasim LS, Sahib IJ. Characterization, modelling, and kinetics studies of the adsorption of phenol from aqueous solutions onto [ZnO/P(AA-CA)] composite as

an adsorbate surface. AIP Conference Proceedings: AIP Publishing; 2023. p. 040002.
70. Sajeesh S, Sharma CP. Mucoadhesive hydrogel microparticles based on poly (methacrylic acid-vinyl pyrrolidone)-chitosan for oral drug delivery. Drug Deliv. 2010;18(4):227-235.
71. Paredes-Laverde M, Silva-Agredo J, Torres-Palma RA. Removal of norfloxacin in deionized, municipal water and urine using rice (Oryza sativa) and coffee (Coffea arabica) husk wastes as natural adsorbents. J Environ Manage. 2018;213:98-108.
72. Paredes-Laverde M, Salamanca M, Silva-Agredo J, Manrique-Losada L, Torres-Palma RA. Selective removal of acetaminophen in urine with activated carbons from rice (Oryza sativa) and coffee (Coffea arabica) husk: Effect of activating agent, activation temperature and analysis of physical-chemical interactions. Journal of Environmental Chemical Engineering. 2019;7(5):103318.
73. Kianipour S, Razavi FS, Hajizadeh-Oghaz M, Abdulsahib WK, Mahdi MA, Jasim LS, et al. The synthesis of the P/N-type $NdCoO_3$/g-$C_3N_4$ nano-heterojunction as a high-performance photocatalyst for the enhanced photocatalytic degradation of pollutants under visible-light irradiation. Arabian Journal of Chemistry. 2022;15(6):103840.
74. Liu Y, Zheng Y, Wang A. Enhanced adsorption of Methylene Blue from aqueous solution by chitosan-g-poly (acrylic acid)/vermiculite hydrogel composites. Journal of Environmental Sciences. 2010;22(4):486-493.
75. Vigneshwaran S, Sirajudheen P, Karthikeyan P, Meenakshi S. Fabrication of sulfur-doped biochar derived from tapioca peel waste with superior adsorption performance for the removal of Malachite green and Rhodamine B dyes. Surfaces and Interfaces. 2021;23:100920.
76. Shaikh WA, Islam RU, Chakraborty S. Stable silver nanoparticle doped mesoporous biochar-based nanocomposite for efficient removal of toxic dyes. Journal of Environmental Chemical Engineering. 2021;9(1):104982.
77. Bhattacharyya A, Banerjee B, Ghorai S, Rana D, Roy I, Sarkar G, et al. Development of an auto-phase separable and reusable graphene oxide-potato starch based cross-linked bio-composite adsorbent for removal of methylene blue dye. Int J Biol Macromol. 2018;116:1037-1048.
78. Nakhjiri MT, Bagheri Marandi G, Kurdtabar M. Adsorption of Methylene Blue, Brilliant Green and Rhodamine B from Aqueous Solution Using Collagen-g-p(AA-co-NVP)/$Fe_3O_4$@$SiO_2$ Nanocomposite Hydrogel. Journal of Polymers and the Environment. 2019;27(3):581-599.